RIETVELD ANALYSIS AND MEM-BASED WHOLE-PATTERN FITTING UNDER PARTIAL PROFILE RELAXATION

FUJIO IZUMI

National Institute for Research in Inorganic Materials, 1-1 Namiki, Tsukuba, Ibaraki 305-0044, Japan

The latest version of a Rietveld-analysis program RIETAN-2000 has a couple of advanced features: partial profile relaxation and whole-pattern fitting based on a maximum-entropy method (MEM). Partial profile relaxation means that primary profile parameters of (nearly) isolated reflections can be individually refined independently of secondary profile parameters. It was combined with split profile functions to achieve better fits between observed and calculated patterns, particularly in samples showing anisotropic profile broadening and reflections with very small d spacings. RIETAN-2000 and an MEM program MEED were integrated into a structure-refinement system named REMEDY. With REMEDY, the pattern calculated from structure factors obtained by MEM analysis is fit to the whole observed pattern. Observed structure factors estimated at the end of the whole-pattern fitting are analyzed again by the MEM. Whole-pattern fitting and MEM analyses are alternately repeated until R factors in the former no longer decrease. Some examples of applying this methodology to structure refinements are introduced.

1. Introduction

The Rietveld method [1] has been extensively used as a leading technique for refining structure parameters of a variety of metal and inorganic compounds. The severe overlap of reflections in the high-Q region ($Q = |\boldsymbol{Q}| = 2\pi/d$; $\boldsymbol{Q}$: scattering vector, d: lattice-plane spacing) in powder diffraction patterns limits the quality and amount of structural information extractable from them in comparison with single-crystal data. However, advances in synchrotron X-ray powder diffraction [2] and time-of-flight (TOF) neutron powder diffraction in recent years have enhanced the resolution, $\Delta d/d$, pronouncedly, enabling us to determine very complex structures whose analyses were formerly difficult with powder data.

Five years have passed since a Rietveld-analysis program RIETAN [3] was introduced in the well-known book entitled "The Rietveld Method." RIETAN has two versions for angle-dispersive diffraction [3, 4] and TOF neutron diffraction [5]. It has been widely utilized, particularly in Japan, contributing to a large number of structural studies. For example, the

structures of the first High-T_c superconductors with fluorite and carbonate blocks were solved with RIETAN for TOF neutron diffraction [6]. This article reviews recent advances in RIETAN with a focus on our original technology: partial profile relaxation [7–9] and whole-pattern fitting based on a maximum-entropy method (MEM) [8, 10].

2. Partial Profile Relaxation

The profile function used in whole-pattern fitting (w.p.f.) generally contains two levels of profile parameters: primary profile parameter (PPP) and, in its turn, secondary profile parameter (SPP). The dependence of a PPP on θ (angle-dispersive diffraction) or d (TOF neutron diffraction) is represented with a physical foundation or in an empirical way in equations including SPP's. For example, the full-width-at-half-maximum (FWHM), H, in the famous equation of Caglioti *et al.* [11]

$$H = \left(U \tan^2 \theta_k + V \tan \theta_k + W\right)^{1/2}, \tag{1}$$

is a PPP specific for reflection k with a Bragg angle of θ_k while U, V, and W are SPP's common to the whole 2θ (d) range. We refine not PPP's but SPP's in the least-squares fitting of whole powder patterns. Such an equation imposes a kind of an equality constraint on a PPP, often failing to describe the relation between the PPP and θ_k (d_k) satisfactorily. As the PPP deviates from the equation relating it to θ_k (d_k), the goodness-of-fit gets worse and worse. The resulting misfit gives rise to serial correlation committing a prerequisite of Gaussian distribution of residuals in least-squares methods.

We have devised an original technique called partial profile relaxation [7–9], where PPP's of (nearly) isolated reflections specified by the user are locally refined independently of their SPP's. In Rietveld analysis under partial profile relaxation, the PPP's of these reflections are all or partially freed from equations relating the PPP's to θ_k (d_k) and diffraction indices, hkl. On the other hand, peak positions and integrated intensities for the relaxed reflections are respectively calculated from lattice and structure parameters in the same fashion as those for the other reflections. Part of the PPP's may be constrained by the equations applied to reflections not to be relaxed. Though the profiles of only low-Q reflections can be substantially relaxed except for very simple structures, better fits in this region necessarily lead to an improvement in the overall fit.

Partial profile relaxation stemmed from a simple idea but is well suited to samples showing anisotropic profile broadening and reflections with very large d values. It is sound and powerful in the point that neither assumption nor approximation is required in regard to the dependence of the PPP's on θ_k (d_k). The profile-relaxation technology allows us to fit more flexible profile functions to observed profiles of relaxed reflections to improve the goodness-of-fit. It can be introduced not only into Rietveld analysis but into pattern decomposition such

as Pawley [12] and Le Bail [13] refinements. Integrated intensities are refined in the Pawley method and calculated after each cycle of least-squares fitting by Rietveld's procedure (refer to Subsection 4.2) [1] in the La Bail method.

The latest version RIETAN-2000 for angle-dispersive diffraction has grown into a versatile program supporting whole-pattern fitting under partial profile relaxation by the Rietveld, Le Bail, and maximum-entropy methods; Le Bail refinement under partial profile relaxation will be published elsewhere. In each of these pattern-fitting methods, three methods of nonlinear least squares can be used: Gauss-Newton, Fletcher's modified Marquardt, and Powell's direction set methods [3, 4]. Powell's method has proved to be most effective for escaping from local minima in the three kinds of pattern fitting.

3. Rietveld Analysis under Partial Profile Relaxation

3.1 Three Split Profile Functions

Partial profile relaxation was first implemented in the Rietveld-analysis program for TOF neutron powder diffraction data measured on the Vega diffractometer at the KENS pulsed neutron source [5, 7]. Later, we made it possible to analyze angle-dispersive diffraction data by whole-pattern fitting under partial profile relaxation [8, 9]. For this purpose, profile relaxation was combined with two split profile functions of Toraya [14]: a pseudo-Voigt function

$$f(x) = \frac{(1+A)\left[\eta_{\mathrm{H}} + \sqrt{\pi \ln 2}(1-\eta_{\mathrm{H}})\right]}{\eta_{\mathrm{L}} + \sqrt{\pi \ln 2}(1-\eta_{\mathrm{L}}) + A\left[\eta_{\mathrm{H}} + \sqrt{\pi \ln 2}(1-\eta_{\mathrm{H}})\right]} \times$$

$$\left\{ \eta_{\mathrm{L}} \frac{2}{\pi H}\left[1 + \left(\frac{1+A}{A}\right)^2 \left(\frac{x}{H}\right)^2\right]^{-1} + (1-\eta_{\mathrm{L}}) \left(\frac{\ln 2}{\pi}\right)^{1/2} \frac{2}{H} \exp\left[-\ln 2 \left(\frac{1+A}{A}\right)^2 \left(\frac{x}{H}\right)^2\right] \right\} \quad (2)$$

and a Pearson VII function

$$f(x) = \frac{2(1+A)}{\sqrt{\pi} H}\left[\frac{A\Gamma(m_{\mathrm{L}} - 1/2)}{\sqrt{2^{1/m_{\mathrm{L}}} - 1}\,\Gamma(m_{\mathrm{L}})} + \frac{\Gamma(m_{\mathrm{H}} - 1/2)}{\sqrt{2^{1/m_{\mathrm{H}}} - 1}\,\Gamma(m_{\mathrm{H}})}\right]^{-1} \times$$

$$\left[1 + \left(2^{1/m_{\mathrm{L}}} - 1\right)\left(\frac{1+A}{A}\right)^2 \left(\frac{x}{H}\right)^2\right]^{-m_{\mathrm{L}}} \quad (3)$$

normalized in such a way that

$$\int_{-\infty}^{+\infty} f(x)\mathrm{d}x = 1. \quad (4)$$

In Eqs. (2) and (3), $x = 2\theta_i - 2\theta_k$, $2\theta_i$ is the diffraction angle at the ith step, A is the asymmetry

parameter, η is the fraction of the Lorentzian component, H is the FWHM expressed as a function of θ_k with Eq. (1), m is the decay parameter, and Γ is the gamma function. Subscripts L and H are regions of 2θ lower and higher than the peak position, respectively. Both equations are effective in the region $x < 0$. For $x > 0$, subscripts L and H should be replaced with each other, and A with $1/A$. These split functions were combined with partial profile relaxation because of their high flexibility.

The dependence of PPP's other than H in Eqs. (2) and (3) on θ_k is empirically expressed in

$$A = A_0 + A_1\left(\sqrt{2} - 1/\sin\theta_k\right) + A_2\left(2 - 1/\sin^2\theta_k\right), \tag{5}$$

$$\eta = \eta_0 + \eta_1(2\theta_k), \tag{6}$$

$$m = -1.517 + 0.980\left[m_0 + m_1(2\theta_k)\right] + 1.578/\left[m_0 + m_1(2\theta_k)\right], \tag{7}$$

where A_0, A_1, A_2, η_0, η_1, m_0, and m_1 are SPP's, namely, refinable parameters in whole-pattern fitting. Two sets of PPP's are assigned to the low- and high-angle sides of each diffraction profile.

Extending Eq. (2) by assigning different FWHM's, H_1 and H_2, to the Lorentzian and Gaussian components, respectively, we have

$$f(x) = \frac{(1+A)\left[\eta_H + \sqrt{\pi\ln 2}(1-\eta_H)\right]}{\eta_L + \sqrt{\pi\ln 2}(1-\eta_L) + A\left[\eta_H + \sqrt{\pi\ln 2}(1-\eta_H)\right]} \times$$

$$\left\{\eta_L \frac{2}{\pi H_1}\left[1+\left(\frac{1+A}{A}\right)^2\left(\frac{x}{H_1}\right)^2\right]^{-1} + (1-\eta_L)\left(\frac{\ln 2}{\pi}\right)^{1/2}\frac{2}{H_2}\exp\left[-\ln 2\left(\frac{1+A}{A}\right)^2\left(\frac{x}{H_2}\right)^2\right]\right\}. \tag{8}$$

This modified split pseudo-Voigt function [8, 9] may be fit to observed profiles of only relaxed reflections. It is flexible enough to fit highly asymmetric profiles in low-2θ regions.

3.2 Examples of Profile-Relaxed Rietveld Refinements

Profile asymmetry mainly arising from axial divergence [15] is pronounced in the Bragg-Brentano geometry and constant-wavelength neutron diffraction. It may be inadequately approximated with symmetric profile functions made asymmetric by various procedures. Flat-specimen and specimen-transparency errors in the parafocusing geometry [15] are particularly difficult to represent analytically. With profile-relaxed Rietveld refinement, we have been successfully analyzing the crystal structures of various zeolites exhibiting reflections in 2θ regions lower than 20° [9, 16, 17].

Figure 1 exemplifies low-2θ parts of Rietveld-refinement patterns for a zeolite, hydrated

Na-LTA (Linde Type A) [9]. Its X-ray powder diffraction data were measured with two Bragg-Brentano-type goniometers: (a) a commercial goniometer with an aperture angle of Soller slits 5° and (b) a newly designed goniometer with a vertical θ:θ configuration and a pair of long Soller slits with an aperture angle of 1°. Unless otherwise stated, we measured powder diffraction data with CuKα radiation using the latter goniometer in all X-ray diffraction studies that will be described from now on. On relaxation of PPP's for five reflections whose indices are noted in this figure, Eq. (8) is fit to extremely asymmetric profiles in (a) and fairly symmetric ones in (b) comparably well. It will also be applicable to intensity data measured by transmission-specimen methods. In what follows, profiles of relaxed reflections will be all expressed in Eq. (8), and those of the other reflections in Eq. (2).

Figure 2 shows observed, calculated, and difference patterns for X-ray Rietveld refinement of hydrated Na-X (faujasite) with 23 sites at general positions [16]. The global minimum could not be reached in the analysis of such a complex structure unless Powell's direction set method [3, 4] were used. PPP's of Eq. (8) were independently refined for 17 reflections to afford very low R factors: R_{wp} = 7.60% (R_e = 5.23%) and R_B = 1.75%. Na^+ ions are situated on framework planes. A large amount of water molecules is incorporated in supercages consisting of 12-membered rings. Each cage is distorted owing to the deviation of an Si:Al amount-of-substance ratio from unity.

Figure 3 demonstrates the result of neutron Rietveld refinement for $AlPO_4$-5 prepared by microwave heating with triethylamine as template molecules [16]. Its intensity data were measured on BT-1 at NIST. Marked incoherent scattering from hydrogen atoms in triethylamine is responsible for the high background. In Rietveld refinement adopting space group *P*6*cc*, we relaxed the PPP's of ten reflections including the highly asymmetric 100 reflection near 10°. Each template molecule with roughly the symmetry of point group C_{3v} is oriented in the so-called head-to-tail manner along the [001] direction. R factors were R_{wp} = 1.83% (R_e = 1.90%) and R_B = 4.25%. Equations representing the dependence of the PPP's on θ_k in Eq. (2), *viz*, Eqs. (1), (5), and (6), were applicable to the neutron diffraction data without any modifications despite their original optimization for the analysis of X-ray diffraction data.

The performance of the conventional and profile-relaxed Rietveld methods in structure refinements of five inorganic materials is embodied in the form of a bar graph, Fig. 4. In the conventional refinements, the pseudo-Voigt function of Thompson, Cox, and Hastings [18] was made asymmetric by a physically meaningful method of expressing the effect of axial divergence on profile shape [19]. Figure 4 reveals that it is far from satisfactory to fit the profile function adopting this pair to observed patterns in spite of its popularity; R_{wp}'s were lowered more or less with Eq. (2) coupled with Eq. (8) for relaxed reflections. The latter combination was particularly effective in zeolites with several reflections in low-2θ regions [9, 16, 17].

4. Whole-Pattern Fitting on the Basis of the MEM

4.1 Background

In single-crystal X-ray analysis, we often carry out difference (D) synthesis, that is, the inverse Fourier transform of differences, $\Delta F_k = F_{ok} - F_{ck}$, between observed structure factors, F_{ok}, and structure factors, F_{ck}, calculated from structure parameters. D synthesis is suitable for detecting subtle differences between real and modeled structures.

Two serious problems hinder the satisfactory application of D synthesis to powder data. One is the appearance of 'ripples' due to the termination effect even in D synthesis where Fourier coefficients with higher orders are regarded as negligible. This effect makes it difficult to extract physically meaningful residual distribution from D-synthesis maps. The other is difficulty in obtaining accurate observed structure factors, $|F_{ok}|$, owing to the collapse of the three-dimensional reciprocal space onto the one-dimensional diffraction pattern.

Sakata *et al.* [20] have been applying the MEM to determination of electron-density distribution with powder diffraction data. In MEM analysis, no model function is fit to the observed pattern unlike Rietveld analysis using least-squares methods [1]; that is, we estimate density distribution whose information entropy is maximized within errors in observed diffraction data. Structural information contained in diffraction data is accordingly extracted by the MEM and reflected on the density map if they have been appropriately measured. Electron densities are calculated from F_{ok}'s in Fourier synthesis. On the other hand, in the MEM, we solve a kind of an inverse problem where electron densities are determined prior to calculation of structure factors, F_{Mk}. The termination effect is, consequently, far less marked in MEM analysis than in Fourier synthesis. Further, the MEM can estimate structure factors of reflections in the high-Q region excluded in the analysis of intensity data; electron densities can therefore be estimated from a limited number of integrated intensities.

The distribution of coherent scattering lengths, b_c, is also determinable by the MEM analysis of neutron diffraction data. For convenience, b_c per unit volume will hereafter be called nuclear density. The term "nuclear density" may be substituted for "electron density" in subsequent general descriptions common to X-ray and neutron diffraction.

4.2 Derivation of Integrated Intensities from Powder Diffraction Data

In the MEM analysis of relatively simple structures with powder diffraction data, $|F_{ok}|$ is usually obtained by pattern decomposition such as individual profile fitting [21], the Pawley method [12], and the Le Bail method [13]. However, most values of $|F_{ok}|$ for compounds exhibiting heavily overlapped reflections can hardly be estimated by pattern decomposition without introducing any structural models.

After Rietveld analysis, the 'observed' integrated intensity, I_{ok}, for reflection k is

approximately computed by apportioning the net diffraction intensity, $y_i - y_b(2\theta_i)$, at step i in the ratio of contributions of overlapping reflections (K = 1, 2, 3, …..) [1]:

$$I_{ok} = \sum_i \left[y_i - y_b(2\theta_i) \right] \frac{Y_{ik}}{\sum_K Y_{iK}}, \tag{9}$$

where y_i is the observed intensity; $y_b(2\theta_i)$ is the background function; Y_{ik} and Y_{iK} are the contributions of reflections k and K to the net diffraction intensity at i, respectively. The summations Σ_i and Σ_K are carried out over all data points contributing to the profile of reflection k and over all the reflections contributing to $y_i - y_b(2\theta_i)$, respectively. In the case of isolated reflections, Eq. (9) reduces to

$$I_{ok} = \sum_i \left[y_i - y_b(2\theta_i) \right]. \tag{10}$$

Consequently, fairly accurate I_{ok} is obtainable in a model-free fashion as long as the background can be adequately approximated by $y_b(2\theta_i)$. Equations (9) and (10) are also used to derive I_{ok} after each cycle in Le Bail refinement [13].

Y_{ik} is evaluated from scale factor s, multiplicity m_k, preferred-orientation factor P_k, Lorentz-polarization factor L_k, structure factor F_{ck}, and profile function $f(x)$:

$$Y_{ik} = s m_k P_k L_k |F_{ck}|^2 f(x). \tag{11}$$

Substituting K for k in this equation yields Y_{iK}. F_{ck} is calculated from structure parameters (occupancies, fractional coordinates, and atomic displacement parameters) in Rietveld analysis. The observed scattering amplitude, $|F_{ok}|$, is determined from

$$|F_{ok}| = \left(\frac{I_{ok}}{s m_k P_k L_k} \right)^{1/2}. \tag{12}$$

Takata *et al.* [22] applied the above procedure to the estimation of $|F_{ok}|$'s analyzed by the MEM. However, *electron densities derived from the $|F_{ok}|$'s are subject to the structural model in Rietveld analysis because Eq. (11) contains F_{ck}*. This undesirable effect enlarges with increasing degree of overlap of reflections, lowering the accuracy of final densities necessarily. The MEM can extract structural details from the $|F_{ok}|$ data estimated in the above way because they involve contributions neglected in the structural model. In addition, $|F_{ok}|$ for an isolated reflection can simply be determined without any structural model, as described earlier. Nevertheless, the dependence of electron-density distribution on the structural model casts a gloom over the combined use of the Rietveld and maximum-entropy methods.

4.3 REMEDY Cycles

To minimize the bias imposed on electron densities by the structural model, we devised

the following iterative procedure [8, 10]:

1. Intensity data are analyzed by the Rietveld method.
2. $|F_{ok}|$'s are approximately evaluated with Eqs. (9)–(12).
3. The $|F_{ok}|$'s with phases, φ, derived from the Rietveld analysis, are analyzed by the MEM to afford three-dimensional electron densities, $\rho(x, y, z)$. Then, F_{Mk} is computed by the Fourier transform of $\rho(x, y, z)$ in the unit cell with a volume of V:

$$F_{Mk} = V\iiint \rho(x,y,z)\exp\left[2\pi \mathrm{i}(hx+ky+lz)\right]\mathrm{d}x\mathrm{d}y\mathrm{d}z. \qquad (13)$$

4. Maps of $\rho(x, y, z)$ are plotted.
5. After checking the electron-density maps, return to step 1 to modify the structural model if necessary.
6. The model function is fit to the whole observed diffraction pattern by refining parameters irrelevant to the crystal structure. Each structure factor in the model function is not calculated from any structure parameters but fixed at F_{Mk}.
7. Terminate unless decreases in R factors in step 6 are significant compared with those in the previous whole-pattern fitting.
8. Return to step 2.

Figure 5 illustrates the above sequence schematically. 'Rietveld', 'MEM', and 'w.p.f.', each in a pair of parentheses, denote analyses whereby structure factors are derived. F_o(Rietveld) and F_o(w.p.f.) in this figure correspond to F_{ok}, and F_c(MEM) is equivalent to F_{Mk}. Contributions of anomalous dispersion to structure factors must be excluded in MEM analysis in the same way as in Fourier synthesis whereas they should be included in whole-pattern fitting. In other words, structure parameters are used only to add anomalous dispersion corrections to structure factors in MEM-based whole-pattern fitting.

Structural details are changed in step 3 while the goodness-of-fit is improved by fixing each structure factor at F_{Mk} in step 6. The effect of the initial structural model on F_{Mk} diminishes with increasing number of iterations. We can therefore approach the final structure reflecting the observed intensity data more closely. Step 6 is not Rietveld analysis but MEM-based whole-pattern fitting to obtain values of F_{ok} containing additional information about structural details. Takata *et al.* [22] utilized not all the processes shown in Fig. 5 but only the part of iterative Rietveld/MEM analyses (inside the upper box consisting of broken lines) for modifying structural models for metallofullerenes, proving its validity and capability.

We have recently developed a state-of-the-art system for MEM-based structure refinement, REMEDY [8, 10], comprising RIETAN for angle-dispersive diffraction [3, 9] and an MEM program MEED [23]. Thus, repetition of MEM analyses and whole-pattern fitting is called REMEDY cycles, as noted in Fig. 5. We have revealed REMEDY to possess a great capacity for determining real structures. Figure 6 is a flow diagram illustrating the normal sequence

of structure refinement with REMEDY and two related programs: Fousyn and Mevius. Fousyn is used for Fourier synthesis, and Mevius for plotting contour maps and calculating fractional coordinates from electron densities. Integers in this figure correspond to step numbers described above. RIETAN provides MEED with structural information, and *vice versa*, through two files storing the F_{ok} and F_{Mk} data.

4.4 Three Reflection Types

The algorithm for the MEM analysis of F_{ok}'s is, *per se*, the same regardless of diffraction procedures. Some special techniques are, however, required to analyze F_{ok}'s derived from powder data. The MEM deals with $|F_{ok}|$'s of reflections whose phases have been estimated by some means. A reflection whose $|F_{ok}|$ is computed from Eqs. (9)–(12) at the end of Rietveld analysis is referred to as a type 1 reflection. F_{ok}'s of overlapped reflections evaluated according to Rietveld's procedure [1] are influenced by the refined structure in a varying degree. Then, the sum of $|F_{ok}|$'s is assigned to a group of overlapped reflections belonging to type 2 to enhance the ability of estimation by the MEM. In the case of type 3 reflections, their peak positions are so near to 2θ(max) that parts of their profiles extend beyond 2θ(max). Nevertheless, we should also calculate the F_{Mk} of a type 3 reflection because excluding them necessarily brings about a bad profile fit near 2θ(max). The F_{Mk} of the type 3 reflection is thus estimated from electron densities determined from only values of F_{ok} for reflections of types 1 and 2. Type 2 reflections are decomposed to afford their individual F_{ok}'s. F_{ok}'s, sums of F_{ok}'s, and only *hkl* indices are output for reflections with types 1, 2, and 3, respectively.

4.5 Structural Data Input/Output by RIETAN and MEED

The estimated standard deviation (e.s.d.), $\sigma(|F_{ok}|)$, of $|F_{ok}|$ for a type 1 reflection is determined from

$$\sigma\left(|F_{ok}|\right) = \frac{|F_{ok}|}{2}\left\{\left[\frac{\sigma(I_{ok})}{I_{ok}}\right]^2 + \left[\frac{\sigma(s)}{s}\right]^2\right\}^{1/2}, \tag{14}$$

where $\sigma(I_{ok})$ and $\sigma(s)$ are the e.s.d.'s of I_{ok} and s, respectively. The sum of $|F_{ok}|$'s, G_o, for a group of type 2 reflections is given by

$$G_o = \left(\frac{\sum_k I_{ok}}{s\sum_k m_k P_k L_k}\right)^{1/2} \tag{15}$$

with the summation Σ_k carried out over all the overlapped reflections. The e.s.d. of G_o is estimated by

$$\sigma(G_{\rm o}) = \frac{G_{\rm o}}{2}\left\{\left[\frac{\sigma\left(\sum_k I_{{\rm o}k}\right)}{\sum_k I_{{\rm o}k}}\right]^2 + \left[\frac{\sigma(s)}{s}\right]^2\right\}^{1/2} \tag{16}$$

analogous to Eq. (14).

At the end of the whole-pattern fitting, I_{ok} is evaluated in a similar manner as Eq. (9):

$$I_{{\rm o}k} = \sum_i \left[y_i - y_{\rm b}(2\theta_i)\right]\frac{Y'_{ik}}{\sum_K Y'_{iK}} \ . \tag{17}$$

Y'_{ik} is the contribution of reflection k to the net diffraction intensity and given by

$$Y'_{ik} = sm_k P_k L_k |F_{{\rm M}k}|^2 f(x), \tag{18}$$

where F_{ck} in Eq. (11) is replaced with $F_{{\rm M}k}$. On substitution of K for k in this equation, we obtain Y'_{iK}. $|F_{ok}|$ and $\sigma(|F_{ok}|)$ are respectively computed with Eqs. (12) and (14) in the same manner as their calculations after the Rietveld analysis [1]. Because overlapped reflections are decomposed during the first MEM analysis without any structural model, they are regarded as type 1 reflections in subsequent processes.

When analyzing neutron diffraction data or X-ray diffraction data for centrosymmetric structures, $|F_{ok}|$ for a profile-relaxed reflection can directly be refined in MEM-based whole-pattern fitting with REMEDY. This unique feature is expected to accelerate the convergence of structure refinement, provided that calculated profiles are in good agreement with observed ones for the relaxed reflections.

4.6 Strategy for Stable Convergence

We should pay attention to electron-density maps obtained from $F_{{\rm M}k}$ data in addition to the convergence test in each iteration. There is particularly a fair chance for structural estimation to be misdirected at the first iteration. Accordingly, we need to repeat steps 2–8 while comparing density maps resulting from MEM analysis with those obtained from F_{ck}'s. This comparison is needed to judge whether the electron-density distribution is affected by the structural model or estimated properly by the MEM. For reflections with unsatisfactory fits between observed and calculated intensities, e.s.d.'s obtained with Eqs. (14) and (16) should appropriately be increased to enhance the degree of freedom in estimation by the MEM; such large residuals usually arise from imperfect representation of the real structure on condition that the intensity data are collected appropriately. If this part were partitioned among overlapped reflections in proportion to their values of Y_{iK}, the MEM would estimate the structure in a way biased in favor of the structural model.

The efficiency of REMEDY cycles depends on the validity of the starting structural model.

If the structure refined in step 1 differs considerably from the real one, MEM analysis may fail in structure refinement owing to the inaccurate partition of observed Bragg intensities among overlapped reflections.

R factors in the whole-pattern fitting are used as the measure of the convergence in REMEDY cycles. *R* factors in model-free MEM analysis are comparable regardless of the progress of the REMEDY cycles because the convergence criterion is a constraint function being equal to unity. Hence, *R* factors in the MEM should not be used to judge the convergence of the iterations.

4.7 Examples of Structure Refinements with REMEDY

The visualization of diffraction data by the MEM is very useful for modifying structural models imperfect with respect to positional disorder, defects, partially occupied sites, *etc*. We investigated the real structure of Na-LTA dehydrated imperfectly with REMEDY [9, 17]. Figure 7 shows electron-density maps plotted for the (110) plane with the vertical axis parallel to the *c* axis. Figures 7(a) and 7(b) were obtained by Rietveld analysis followed by Fourier synthesis and MEM analysis with the same number of F_{ok} data, respectively. 'Ripples' and negative densities dominate the Fourier map because of the termination effect, which makes it virtually impossible to distinguish residual water molecules from ripples in (a). In contrast with (a), such noises are suppressed in (b), so that residual water molecules can be unambiguously detected at four positions indicated by arrows inside a β cage despite an occupancy as low as 0.028. The MEM owes the predominance over Fourier synthesis to its excellent capability to estimate structure factors of reflections whose peak positions exceed 2θ(max).

With REMEDY, the order-disorder-type phase transition of KH_2PO_4 was studied with its neutron powder diffraction data measured on HRPD (λ = 1.16 Å) at JRR-3M [24]. For MEM analysis, we used MEND [25] instead of MEED to deal with hydrogen with a negative b_c of –3.7390 fm. The ferroelectric and paraelectric phases of KH_2PO_4 are stable below and above its Curie temperature of 123 K, respectively. The nuclear-density map plotted for the (001) plane in Fig. 8 resulted from repeating MEM analyses and whole-pattern fitting of the intensity data for the paraelectric phase at room temperature. Hydrogen atoms are statistically distributed at a pair of positions with a distance between the twin peaks of *ca*. 0.36 Å, which is in good agreement with values reported in the literature. On the other hands, a hydrogen atom in the ferroelectric phase at 10 K tends to occupy a single position near to an oxygen atom.

$K_xTi_{2-x/3}Li_{x/3}O_4$ (x = 0.8) contains lepidocrocite-related $Ti_{2-x/3}Li_{x/3}O_4$ layers composed of edge-sharing $(Ti,Li)O_6$ octahedra and charge-balancing K^+ ions in the interlayer domain [26]. Rietveld refinement of $K_xTi_{2-x/3}Li_{x/3}O_4$ with neutron powder diffraction data showed K^+ ions

to be disordered between two $Ti_{2-x/3}Li_{x/3}O_4$ layers. An unreasonably large isotropic atomic displacement parameter, B, of *ca.* 10 Å^2 for K evidently originated in its positional disorder. Conventional Rietveld analysis adopting a split-atom model would fail to express the real structure adequately in such a highly disordered system. Then, X-ray Rietveld refinement of $K_xTi_{2-x/3}Li_{x/3}O_4$ was followed by three iterations of MEM analyses and whole-pattern fitting, which lowered R_{wp} a little from 11.56% to 10.63% (R_e = 10.54%) and R_B dramatically from 5.35% to 1.53% [27]. The striking decrease in R_B must result from better representation of the structural details, particularly the disordered distribution of K^+ ions.

A final electron-density map determined for the (100) plane is plotted in Fig. 9. A winding stream of K^+ ions along the [001] direction was clearly visualized by virtue of the iterative analyses by the MEM and whole-pattern fitting. Positional disordering of K^+ ions is partly ascribable to large differences in the oxidation states and ionic radii between Ti^{4+} and Li^+ ions in six-fold coordination. Thus, our first challenge to the determination of spatial distribution for highly disordered species was quite successful.

We determined nuclear and electron densities in a high-temperature superconductor $HgBa_2CuO_{4+\delta}$ (T_c = 97 K) whose content of carbonate ions was minimized [10, 28]. Its neutron powder diffraction data were collected on HRPD (λ = 1.823 Å) at JRR-3M. In both neutron and X-ray diffraction, structure refinements with REMEDY gave lower R factors than conventional Rietveld analysis. R factors were particularly reduced in X-ray diffraction. No distribution of bonding electrons can be determined by the Rietveld method to refine structure parameters contained in F_{ck}. On the other hand, the MEM enables us to represent chemical bonds by electron densities in a higher degree of freedom, which leads to the close approach of F_{Mk}'s toward F_{ok}'s. In fact, densities of bonding electrons between metal and oxygen varied appreciably during the REMEDY cycles.

Figure 10 displays (a) nuclear and (b) electron densities on the (100) plane of $HgBa_2CuO_{4+\delta}$. Dotted lines denote a and c axes of the tetragonal unit cell. Interposition of bonding electrons between Hg and O2 and between Cu and O1, and nearly electrostatic interaction between Cu and O2 are clearly seen in this figure. Comparison of (a) with (b) shows that thermal vibrations of Cu and Hg predominate along the [001] direction perpendicular to the CuO_2 sheet and on the z = 0 plane perpendicular to an $[O2–Hg–O2]^{2-}$ ion, respectively. These findings are reasonable considering the highly covalent character of the Cu–O1 and Hg–O2 bonds. Although harmonic thermal motion was assumed in the Rietveld analysis prior to the REMEDY cycles, isosurfaces of nuclear densities for O2 considerably differed from ellipsoids. In fact, the analysis of anharmonic thermal vibration for O2 gave significant cubic and quartic anharmonic terms [25].

Interstitial oxygen defects, O3, at (1/2, 1/2, 0) are responsible for hole doping in $HgBa_2CuO_{4+\delta}$. In conventional Rietveld analysis, B for a slightly occupied site like O3 is

arbitrarily fixed at a typical value, *e.g.*, 1 Å^2, to refine only its occupancy, *g*, on account of very high correlation between *B* and *g*. We took more elaborate approaches to obtain more reliable values of *g*(O3) and *B*(O3). That is, *g*(O3) was estimated at 0.14 by integrating nuclear densities of O3, and *B*(O3) at 1.5 Å^2 by evaluating mean square displacements. This technique can generally be used to advantage in the determination of *B* and *g* for sites occupied partially.

5. Closing Remarks

We have been routinely introducing partial profile relaxation into most of our Rietveld refinements with angle-dispersive X-ray and neutron diffraction data [9, 16, 17, 24, 27] and TOF neutron diffraction data [7, 8, 28]. This technique more or less surpasses the conventional Rietveld method in goodness-of-fit, improving accuracy in structure parameters with better estimation of e.s.d.'s. It is also useful when combined with MEM-based whole-pattern fitting [10, 24, 27, 28]. To minimize the influence of the structural model in Rietveld analysis on final densities determined with REMEDY, the goodness-of-fit must reach a very high level; this can easily be accomplished with partial profile relaxation. At present, REMEDY cycles would not function well in practice without this feature.

REMEDY is eminently suitable for

1. modifying imperfect structural models for Rietveld analysis through the visualization of intensity data [17, 22],
2. modeling chemical bonds, nonlocalized electrons, and anharmonic thermal motion [10, 28],
3. analyzing the crystal structure of a compound with a highly disordered atomic configuration [27].

The first application serves the construction of structural models [17, 22]; diffraction intensities scattered in the reciprocal space are converted into electron densities filling the real space. The second and third applications are attainable more satisfactorily with REMEDY than with programs for conventional Rietveld analysis because *crystal structures are represented not by structure parameters but by three-dimensional electron/nuclear densities on the use of REMEDY*. Of course, X-ray and neutron diffraction should be utilized for (a) the more adequate expression of chemical bonds and (b) the analysis of anharmonic thermal vibration and disordered structures, respectively.

REMEDY is a newborn system that needs to be tested and polished up further. We will apply it to a variety of compounds to improve its methodology and confirm its great capability.

Acknowledgments

The encouragement and support of S. Kumazawa, T. Ikeda, and A. Yamamoto during the

present work are gratefully appreciated. Thanks are also due to T. Sasaki and W.-Z. Hu for technical assistance in the synthetic work, and Q. Huang and K. Oikawa for the neutron diffraction experiments.

References

[1] H. M. Rietveld, *J. Appl. Crystallogr.*, **2**, 65 (1969).

[2] D. E. Cox, "Synchrotron Radiation Crystallography," ed by P. Coppens, Academic Press, London (1992), Chap. 9.

[3] F. Izumi, "The Rietveld Method," ed by R. A. Young, Oxford University Press, Oxford (1995), Chap. 13.

[4] F. Izumi, "Applications of Synchrotron Radiation to Materials Analysis," ed by H. Saisho and Y. Gohshi, Elsevier, Amsterdam (1996), Chap. 7.

[5] F. Izumi, H. Asano, H. Murata, and N. Watanabe, *J. Appl. Crystallogr.*, **20**, 411 (1987).

[6] F. Izumi, *Trans. Am. Crystallogr. Assoc.*, **29**, 11 (1993).

[7] T. Ohta, F. Izumi, K. Oikawa, and T. Kamiyama, *Physica B (Amsterdam)*, **234–236**, 1093 (1997).

[8] F. Izumi, S. Kumazawa, T. Ikeda, and T. Ida, "Powder Diffraction," ed by S. P. Sen Gupta, Allied Publishers, New Delhi (1998), pp. 24–36.

[9] F. Izumi and T. Ikeda, *Mater. Sci. Forum*, **321–324**, 198 (2000).

[10] F. Izumi, S. Kumazawa, T. Ikeda, W.-Z. Hu, A. Yamamoto, and K. Oikawa, *Mater. Sci. Forum*, in press.

[11] G. Caglioti, A. Paoletti, and F. P. Ricci, *Nucl. Instrum. Methods*, **35**, 223 (1958).

[12] G. S. Pawley, *J. Appl. Crystallogr.*, **14**, 357 (1981).

[13] A. Le Bail, H. Duroy, and J. L. Fourquet, *Mater. Res. Bull.*, **23**, 447 (1988).

[14] H. Toraya, *J. Appl. Crystallogr.*, **23**, 485 (1990).

[15] W. Parrish, "International Tables for Crystallography," Vol. C, ed by A. J. C. Wilson, Kluwer, Dordrecht (1992), pp. 42–79.

[16] T. Ikeda, K. Miyazawa, F. Izumi, Q. Huang, and A. Santoro, *J. Phys. Chem. Solids*, **60**, 1531 (1999).

[17] T. Ikeda, F. Izumi, T. Kodaira, and T. Kamiyama, *Chem. Mater.*, **10**, 3996 (1998).

[18] P. Thompson, D. E. Cox, and J. B. Hastings, *J. Appl. Crystallogr.*, **20**, 79 (1987).

[19] L. W. Finger, D. E. Cox, and A. P. Jephcoat, *J. Appl. Crystallogr.*, **27**, 892 (1994).

[20] M. Sakata, R. Mori, S. Kumazawa, M. Takata, and H. Toraya, *J. Appl. Crystallogr.*, **23**, 526 (1990).

[21] H. Toraya, "The Rietveld Method," ed by R. A. Young, Oxford University Press, Oxford (1995), Chap. 14.

[22] M. Takata, B. Umeda, E. Nishibori, M. Sakata, Y. Saito, M. Ohno, and H. Shinohara,

Nature (London), **377**, 46 (1995).

[23] S. Kumazawa, Y. Kubota, M. Takata, M. Sakata, and Y. Ishibashi, *J. Appl. Crystallogr*., **26**, 453 (1993).

[24] S. Kumazawa, S. Yamamura, E. Nishibori, M. Takata, M. Sakata, F. Izumi, and Y. Ishii, *J. Phys. Chem. Solids*, **60**, 1407 (1999).

[25] S. Kumazawa, M. Takata, and M. Sakata, *Acta Crystallogr*., *Sect. A*, **51**, 651 (1995).

[26] T. Sasaki, F. Kooli, M. Iida, Y. Michiue, S. Takenouchi, Y. Yajima, F. Izumi, B. C. Chakoumakos, and M. Watanabe, *Chem. Mater*., **10**, 4123 (1998).

[27] F. Izumi, T. Ikeda, T. Sasaki, and S. Kumazawa, *Mol. Cryst. Liq. Cryst*., in press.

[28] F. Izumi, A. Yamamoto, N. R. Khasanova, S. Kumazawa, W.-Z. Hu, and T. Kamiyama, *Physica C (Amsterdam)*, in press.

Figure captions

Fig. 1. Observed (plus marks), calculated (solid line), and difference (bottom) patterns of Na-LTA in a low-2θ region. X-Ray diffraction data were measured with CuKα and a pair of Soller slits having angular apertures of (a) 5° and (b) 1°.

Fig. 2. Rietveld-refinement patterns for hydrated Na-X. The X-ray diffraction pattern between 9° and 35° is magnified in the inset.

Fig. 3. Observed, calculated, and difference patterns for $AlPO_4$-5 incorporating triethylamine (λ = 2.0785 Å). The neutron diffraction pattern between 33° and 90° is magnified in the inset.

Fig. 4. R_{wp}'s (%) resulting from conventional and profile-relaxed Rietveld refinements of five inorganic compounds. KTLO: $K_xTi_{2-x/3}Li_{x/3}O_4$ (x = 0.8), Apatite: $Ca_5(PO_4)_3F$. Synchrotron X-ray diffraction data were measured with a wavelength of 0.9997 Å for Nd_2CuO_4 while CuKα radiation was used for the other compounds.

Fig. 5. Flow chart of structure refinement by Rietveld analysis followed by iterative MEM-based whole-pattern fitting.

Fig. 6. Programs and files used in Rietveld analysis, MEM-based whole-pattern fitting, and Fourier synthesis.

Fig. 7. Electron-density distribution on the (110) section in dehydrated Na-LTA. (a) Fourier synthesis, range: –1 to 5 e/Å^3, step: 0.1 e/Å^3. (b) MEM analysis, range: 0.1 to 5 e/Å^3, step: 0.12 e/Å^3.

Fig. 8. Nuclear-density distribution projected on the (001) plane in the paraelectric phase of KH_2PO_4 at room temperature. Contours were plotted for 2.5×1.5^n fm/Å^3 (n = 0–20).

Fig. 9. Electron-density distribution on the (100) section of $K_xTi_{2-x/3}Li_{x/3}O_4$ (x = 0.8). Range: 0.2–8 e/Å^3.

Fig. 10. (a) Nuclear- and (b) electron-density maps of the (100) plane in $HgBa_2CuO_{4+\delta}$. Arrows denote directions along which thermal motion is more significant.

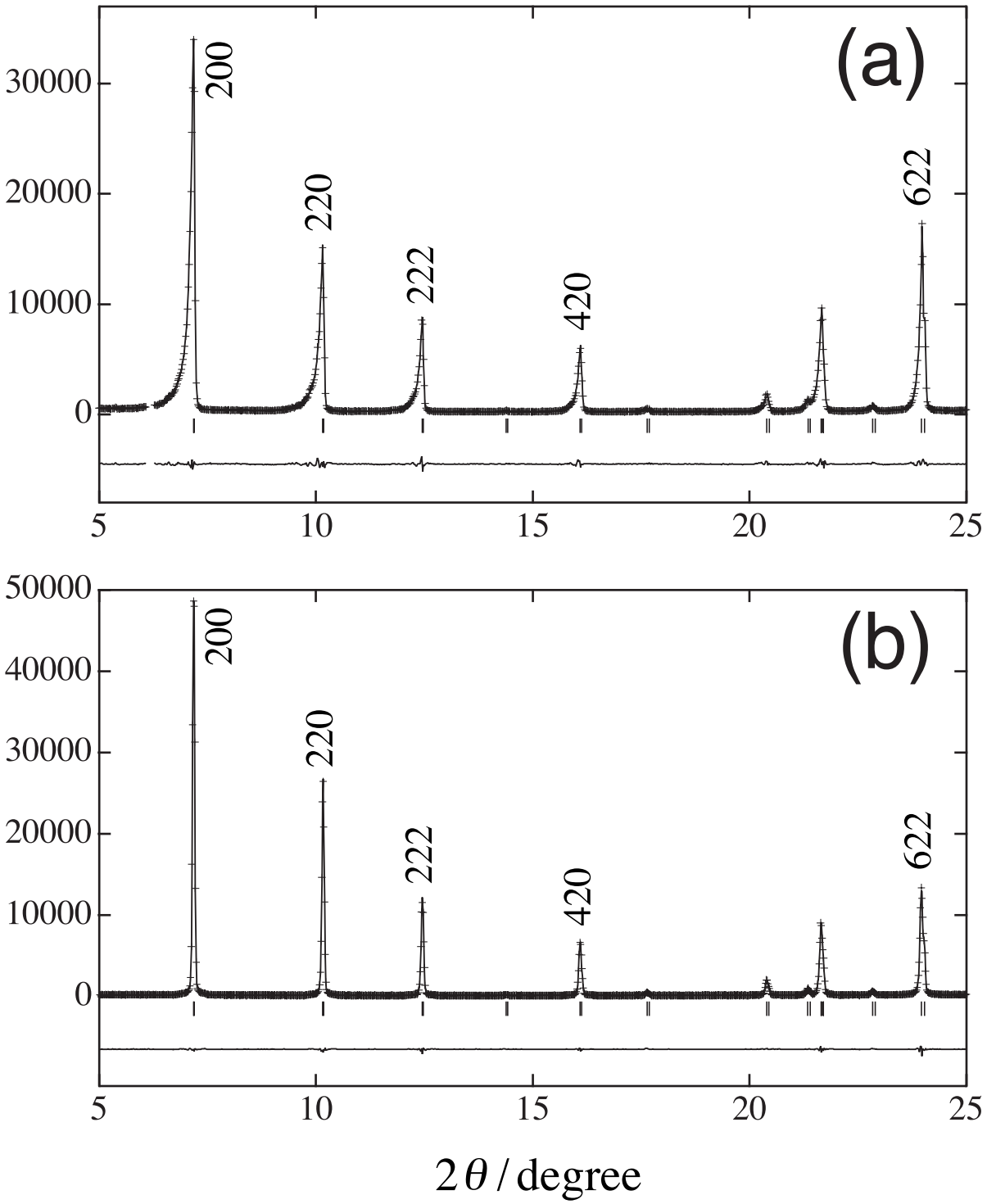
(a)
200
220
222
420
622
30000
20000
10000
0
5
10
15
20
25
(b)
200
220
222
420
622
50000
40000
30000
20000
10000
0
5
10
15
20
25
2θ / degree

Fig. 1

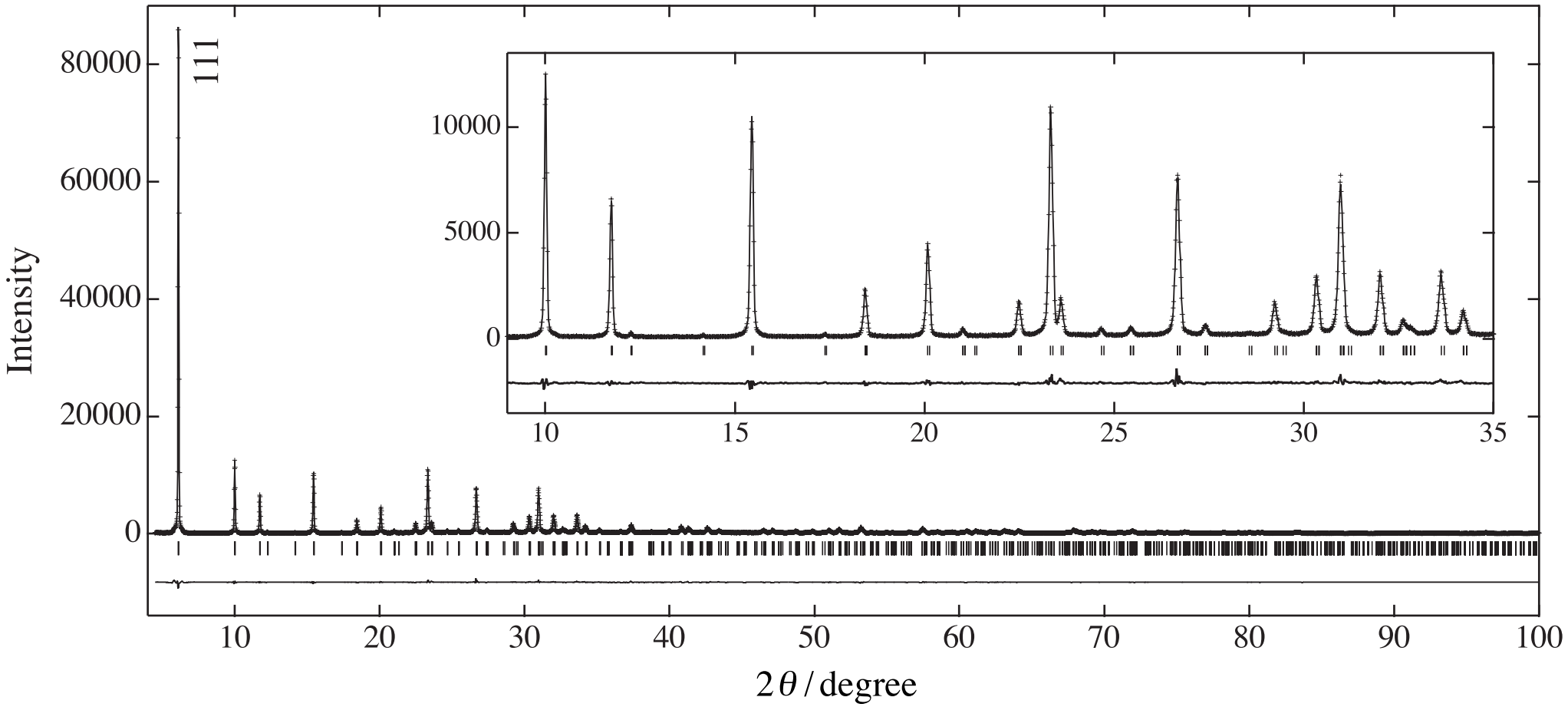
111
Intensity
80000
60000
40000
20000
0
10
20
30
40
50
60
70
80
90
100
2θ / degree
10000
5000
0
10
15
20
25
30
35

Fig. 2

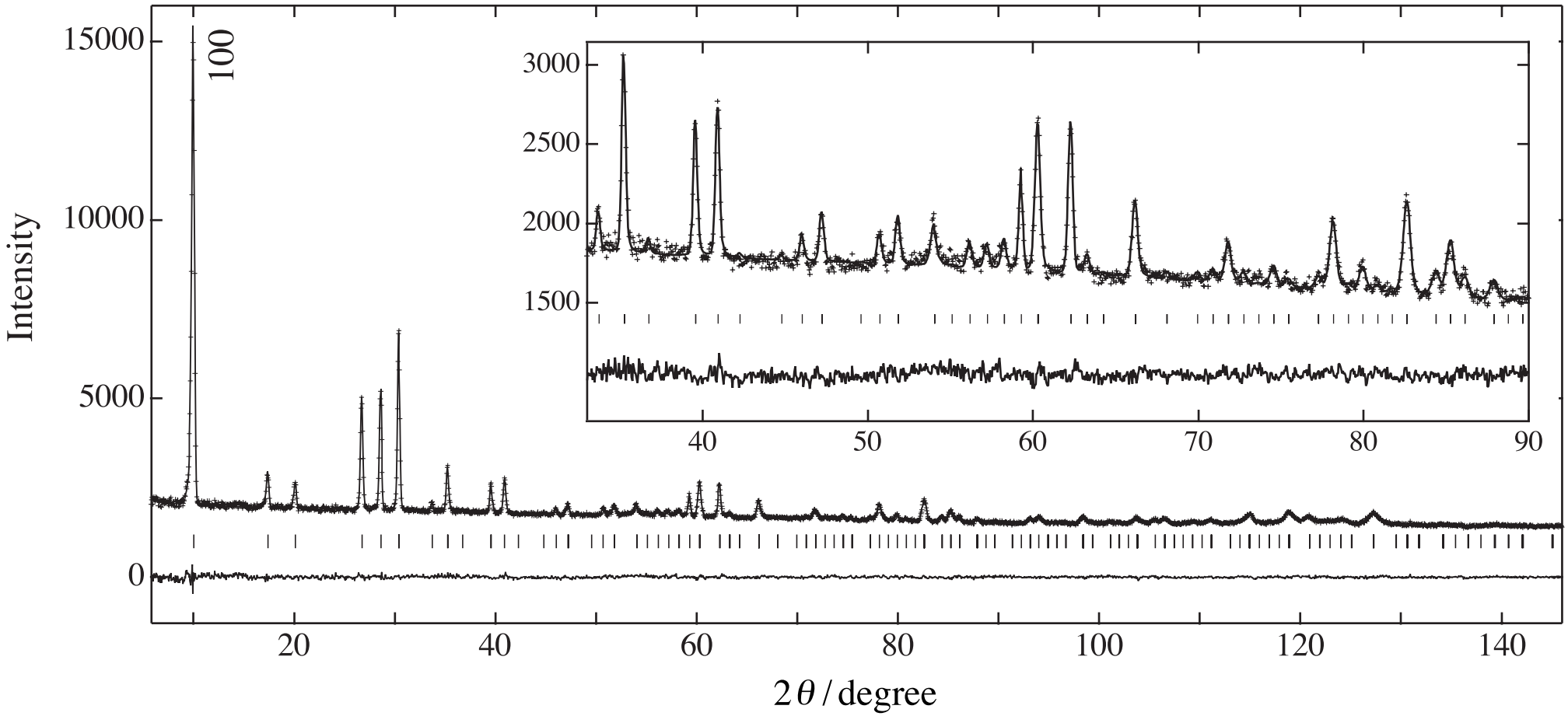
15000
10000
5000
0
Intensity
100
3000
2500
2000
1500
40
50
60
70
80
90
20
40
60
80
100
120
140
2θ / degree

Fig. 3

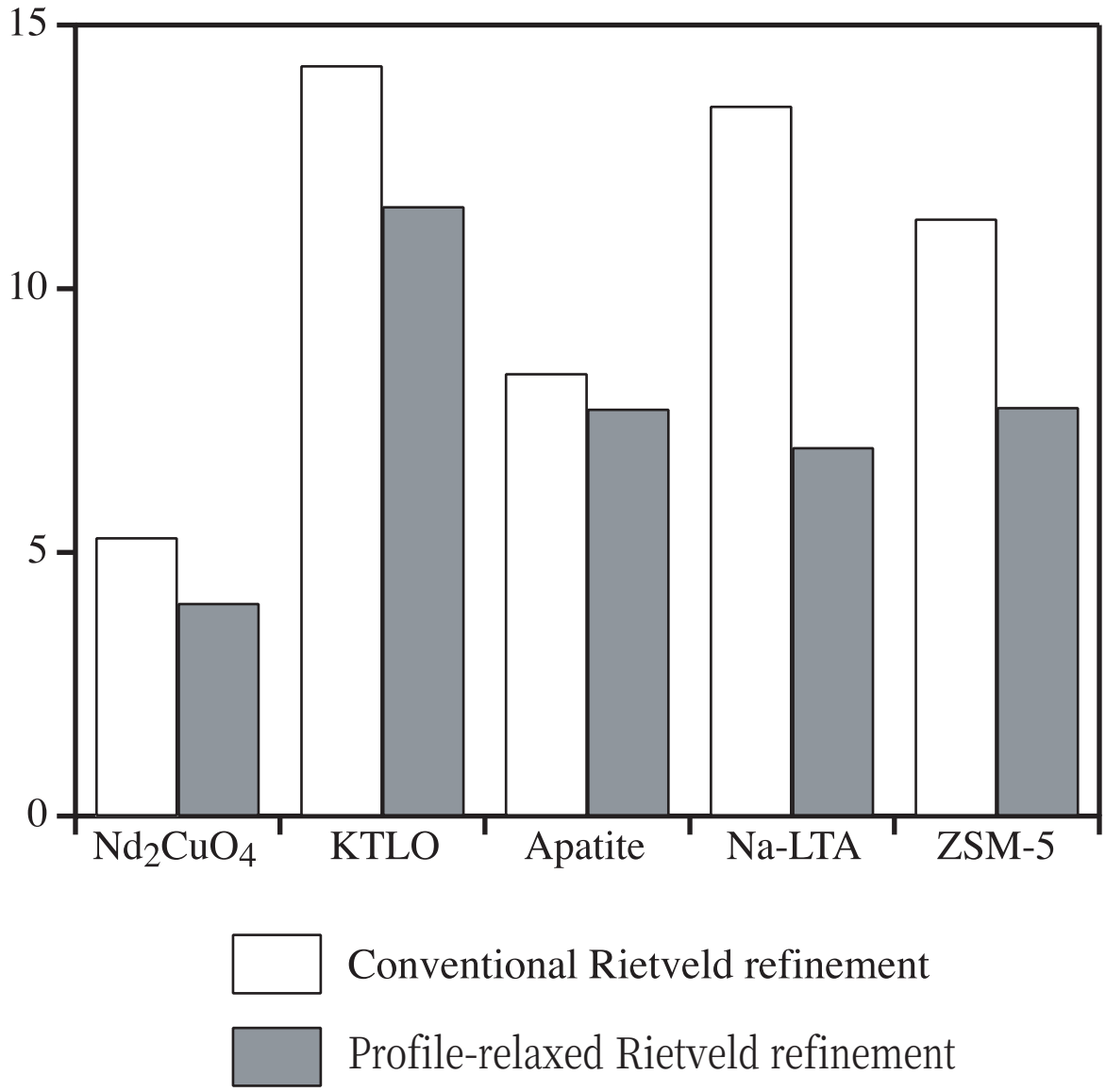
15
10
5
0
Nd2CuO4
KTLO
Apatite
Na-LTA
ZSM-5
Conventional Rietveld refinement
Profile-relaxed Rietveld refinement

Fig. 4

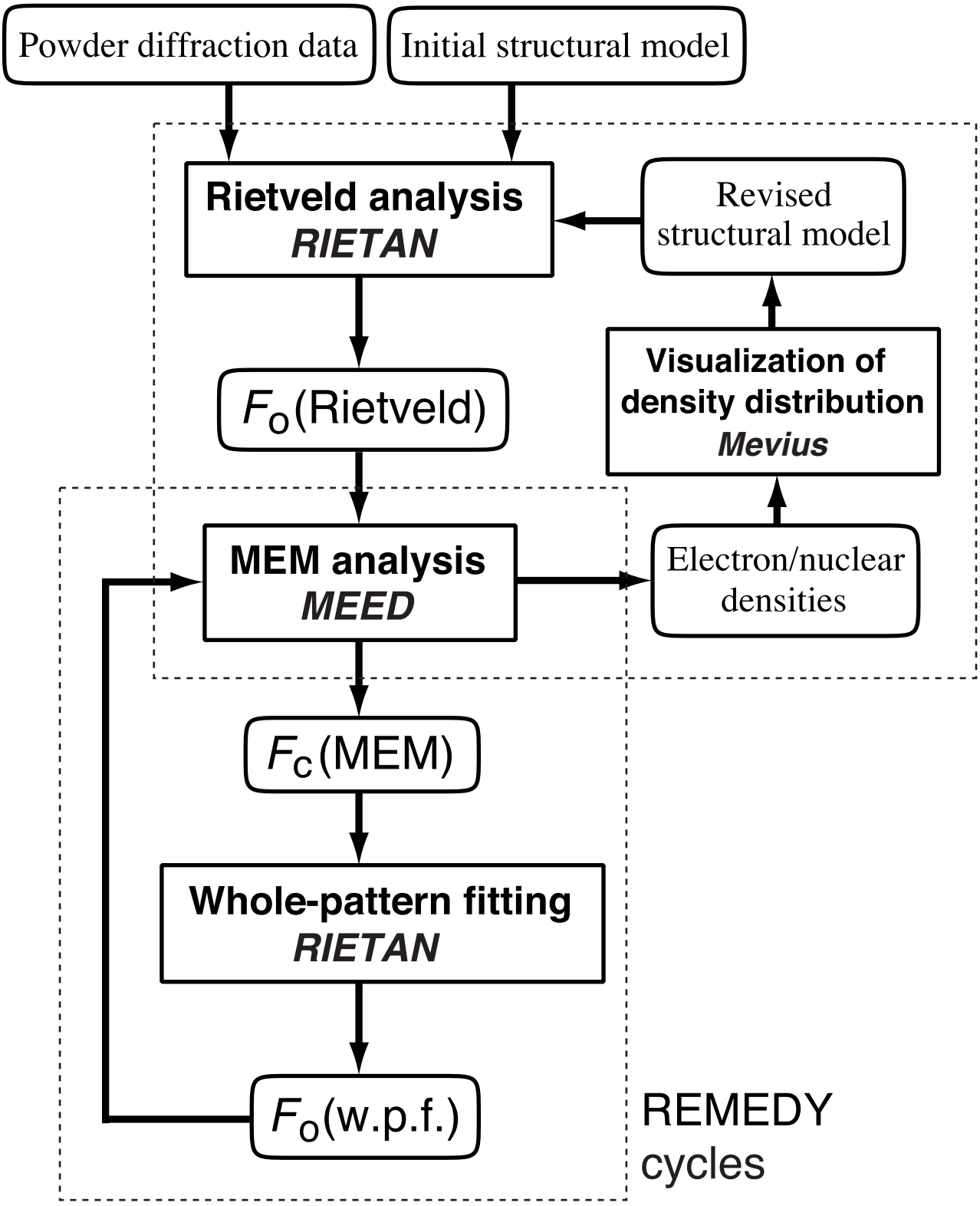
Powder diffraction data
Initial structural model
Rietveld analysis
RIETAN
Revised
structural model
F_o(Rietveld)
Visualization of
density distribution
Mevius
MEM analysis
MEED
Electron/nuclear
densities
F_c(MEM)
Whole-pattern fitting
RIETAN
F_o(w.p.f.)
REMEDY
cycles

Fig. 5

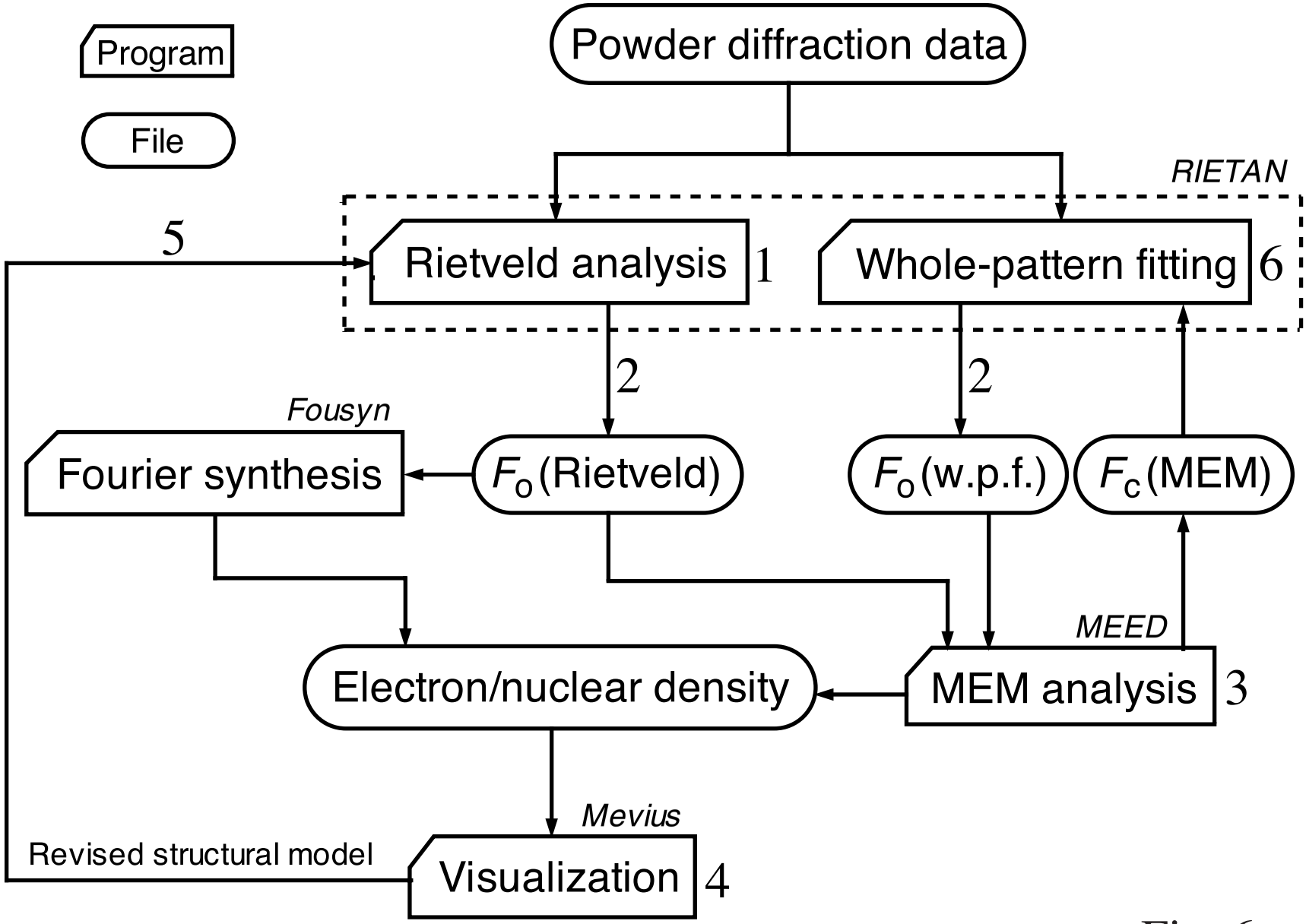
Program
File
Powder diffraction data
RIETAN
5
Rietveld analysis
1
Whole-pattern fitting
6
2
2
Fousyn
Fourier synthesis
F_o(Rietveld)
F_o(w.p.f.)
F_c(MEM)
MEED
Electron/nuclear density
MEM analysis
3
Mevius
Revised structural model
Visualization
4

Fig. 6

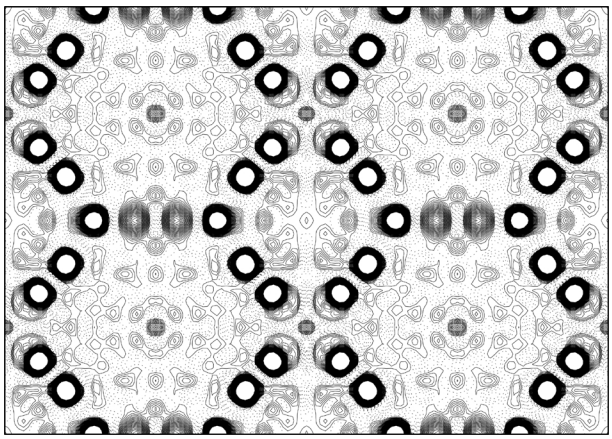

(a)

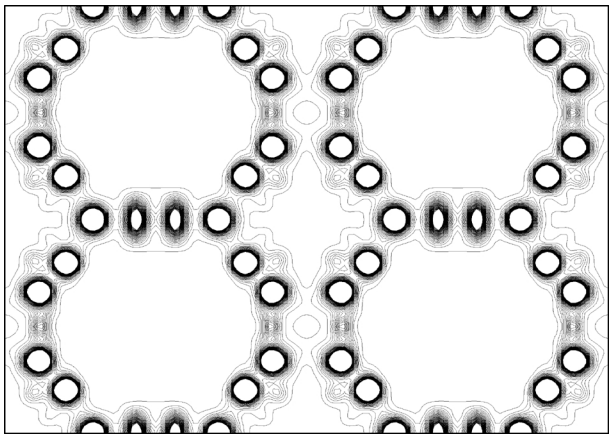

(b)

Fig. 7

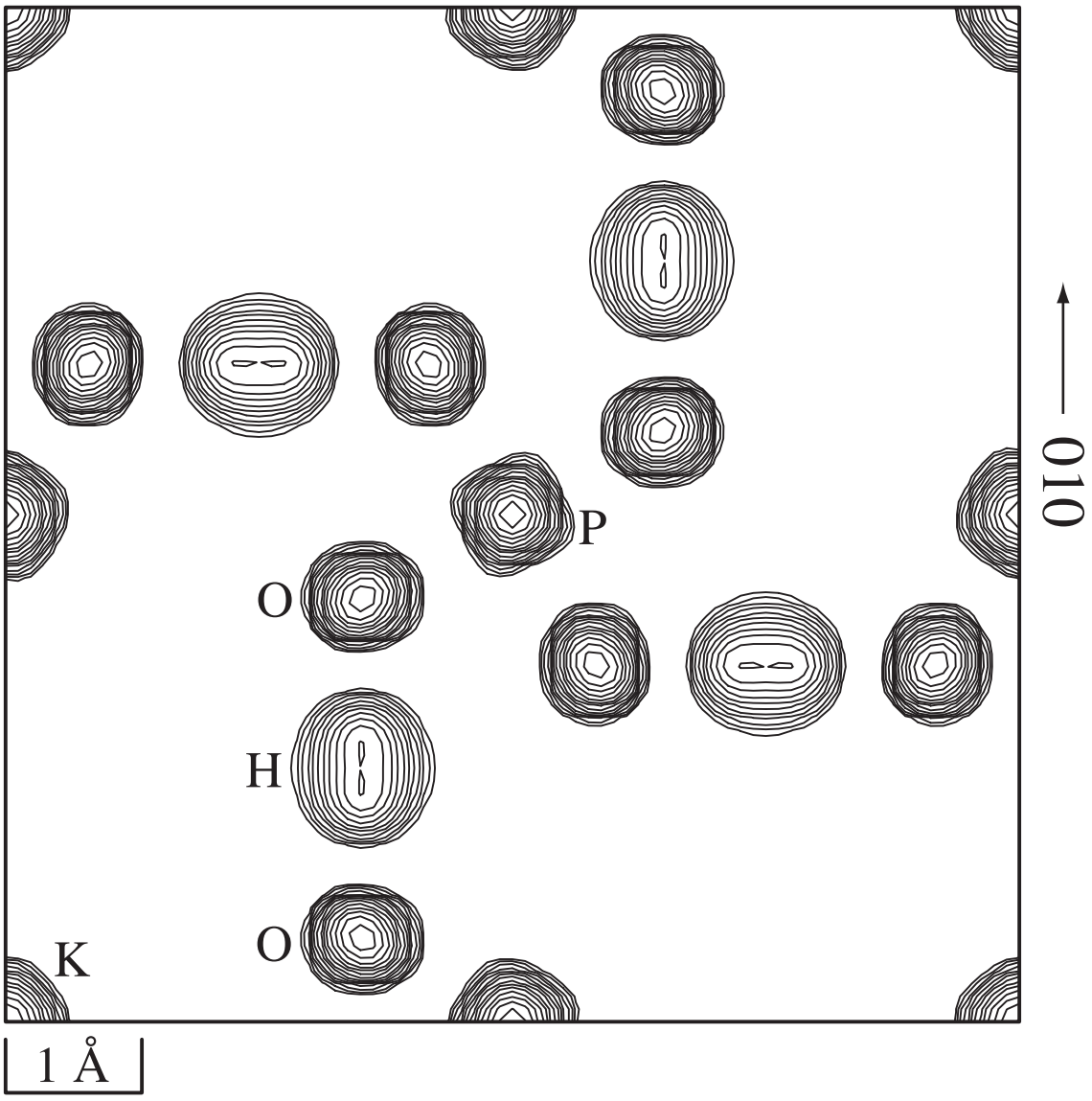

Fig. 8

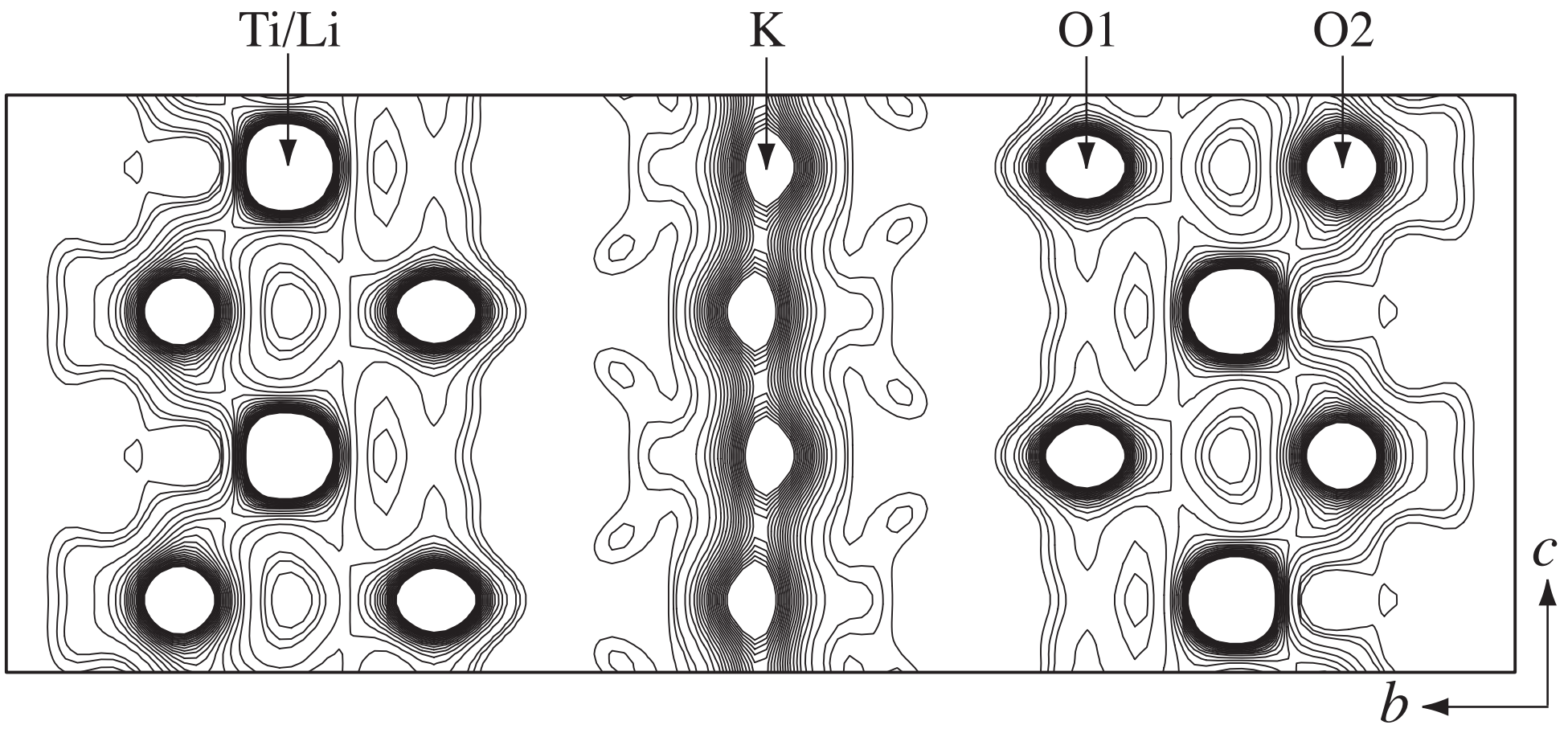

Fig. 9

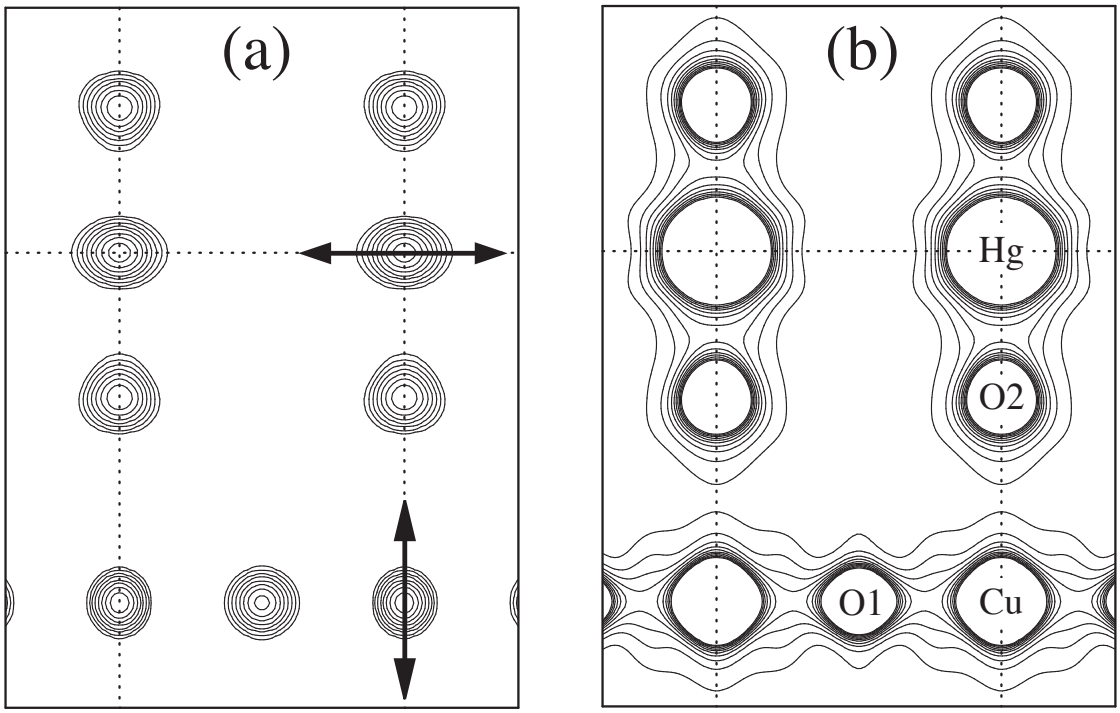

Fig. 10